PHOTODISSOCIATION PATHWAYS OF ACETONE UPON EXCITATION INTO THE 3s RYDBERG STATE: ADIABATIC VERSUS DIABATIC MECHANISM

Ivana ANTOL[a1,*], Mirjana ECKERT-MAKSIĆ[a2], Milan ONČÁK[b1,+], Petr SLAVÍČEK[b2,*,+] and Hans LISCHKA[c,*]

[a] *Division of Organic Chemistry and Biochemistry, Rudjer Bošković Institute, P.O. Box 180, HR-10002 Zagreb, Croatia; e-mail:* [1] *iantol@emma.irb.hr,* [2] *mmaksic@emma.irb.hr*

[b] *Department of Physical Chemistry, Institute of Chemical Technology, Prague, Technická 5, 166 28 Prague 6, Czech Republic; e-mail:* [1] *milan.oncak@vscht.cz,* [2] *petr.slavicek@vscht.cz*

[c] *Institute for Theoretical Chemistry, University of Vienna, Waehringerstrasse 17, A-1090 Vienna, Austria; e-mail: hans.lischka@univie.ac.at*

Received May 29, 2008
Accepted August 19, 2008
Published online December 1, 2008

Dedicated to Professor Rudolf Zahradník on the occasion of his 80th birthday.

Photolysis of acetone upon excitation to the 3s Rydberg excited state has been studied by means of high level ab initio methods. The calculations have been performed on multi-configurational self consistent field (MCSCF) level with a subsequent addition of dynamical correlation both by perturbation theory (CASPT2) and via a configuration interaction expansion up to double excitations (MR-CISD). In addition to the major photoreaction that is well known Norrish type α-cleavage, the formation of hydrogen and acetonyl (1-methyloxy or 2-oxopropyl) radical has been discussed. The major question addressed is whether the dynamical processes occur adiabatically on the S_2 surface or diabatically, with non-adiabatic transitions taking place in the course of the reactions.

Keywords: Ab initio calculations; Acetone; Conical intersections; Deactivation mechanisms; Photochemistry; Photolysis; Reaction mechanism; Radicals; Norrish cleavage.

Photolysis of acetone via α-cleavage (Norrish I type reaction) has been and still is one of the most thoroughly studied photochemical reactions[1–11].

+ Also at: *J. Heyrovský Institute of Physical Chemistry, Academy of Sciences of the Czech Republic, v.v.i., Dolejškova 3, 182 23 Prague 8, Czech Republic.*

doi:10.1135/cccc20081475

One reason for such scientific interest is due to the fact that acetone is the smallest ketone, serving as a prototype for the study of photochemical and photophysical properties of a whole class of carbonyl compounds[3–6]. On the other side there is an ecological interest particularly focused on photochemical reactions in upper layers of the troposphere, where acetone is the most abundant organic non-methane species. There, its chemistry has been shown to be responsible for the HO_x radicals and peroxy acetyl nitrate (PAN) production[7].

After photon absorption, the major photochemical paths of acetone deactivation involve the dissociation of one or two methyl groups:

$$CH_3COCH_3 + h\nu \rightarrow COCH_3 + CH_3$$

$$COCH_3 \rightarrow CO + CH_3$$

Dynamics and molecular mechanism of the overall reaction depends strongly on the excitation wavelengths and the excess energy. Following our recent interest in studying photodeactivation mechanisms in small organic molecules by ab initio dynamics simulations[12], the focus here will be on the excitation of acetone into the Rydberg 3s state (second absorption band in the region of 195–180 nm). In that case the intersystem crossing does not compete with the deactivation via singlet potential surfaces.

It is not the intention of this paper to present a historical overview on the numerous investigations[3–6,8–10] undertaken to provide details on the acetone S_2 photolysis. Instead, a brief summary of the most recent experimental and theoretical results will be given. Based on femtosecond experiments, Chen et al.[9] have proposed the following mechanism:

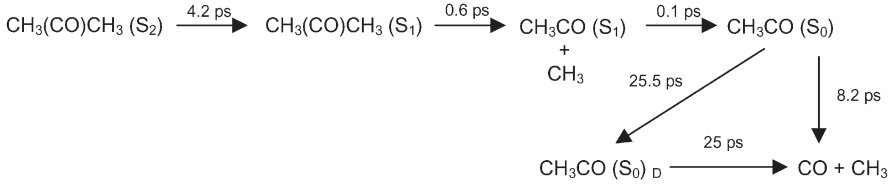

According to this experimentally based proposal, the system relaxes to the S_1 state in about 4 ps after the excitation into the S_2 state. Subsequently, the first methyl radical dissociates after 0.6 ps. The acetyl radical CH_3CO formed in this step converts from the S_1 state into the ground electronic state S_0 within additional 0.1 ps. Dissociation of second CH_3 radical from

hot ground state acetyl intermediate shows a very complex dynamics. This is due to a competition between dissociation from vibrationally excited acetyl radical (that takes 8.2 ps) and very slow intramolecular vibrational energy redistribution (25.5 ps) to localized bending energy in a "dark" CH_3CO $(S_0)_D$ state. It is interesting to note that dissociation of the second methyl radical may be suppressed if a collisional relaxation takes place in the S_1 state[11]. Experimental dynamics studies on acetone are supplemented with experiments on a fully deuterated acetone-d_6. Strong isotope effect is observed: a rate of switching from the S_2 into S_1 state is slowed down by a factor of three[10].

The Norrish cleavage of acetone from S_2 has been thoroughly studied by Zewail and coworkers, experimentally by femtosecond-resolved time of flight mass spectrometry and theoretically by CASSCF and TD-DFT quantum chemical methods[4]. Based on these studies two mechanisms for the reaction were proposed: (i) Stepwise dissociation of two C–C bonds on the S_2 excited state surface with calculated energy barriers of 0.7 eV and 0.03 eV. (ii) Internal relaxation to the S_1 state where the first C–C bond dissociation takes place. The second C–C bond dissociation in the acetyl radical proceeds on the ground state potential energy surface after very fast S_1/S_0 decay governed by the relaxation to linear S_1 acetyl radical minimum. The S_2/S_1 internal conversion in the parent acetone was proposed to occur via a conical intersection (CI) with a compressed C–O bond lying about 1.2 eV above the S_2 minimum. Since neither the transition state for the direct C–C bond dissociation on the S_2 potential energy surface nor the S_2/S_1 CI are energetically available with 193 nm photon excitation around the origin of the S_2 band, they concluded that a relatively slow internal conversion to the S_1 state probably takes place. If the excitation energy is higher (~8 eV excitation to higher Rydberg states) than the first mechanism is activated after very fast relaxation form higher Rydberg sates to the S_2 (50 fs).

Photoexcitation of acetone in the VUV region opens also minor reaction channels: hydrogen atom dissociation (~3%) and methane formation (<2%)[13,14]. The latter channel results from bimolecular collisions and will not be considered further. Acetonyl radical (alternatively 1-methylvinoxy or 2-oxopropyl radical) formation by photoabstraction of a hydrogen atom from acetone has a quantum yield of 0.039 ± 0.006 [15].

$$CH_3(CO)CH_3\ (S_2) \rightarrow CH_3(CO)CH_2\ (S_0) + H$$

The mechanism of hydrogen abstraction has been investigated theoretically on the ground state and the lowest triplet state of acetone using the

B3LYP/6-311G(d,p) method[15]. An attempt to describe this reaction path on the first excited singlet surface at similar levels of theory (TD-DFT and CIS) failed due to deficiencies in the single reference electron configuration treatment. To the best of our knowledge, theoretical characterization of hydrogen atom cleavage from acetone upon excitation to both the S_1 and the S_2 states has not been reported as yet.

In this paper, we explore the photochemistry of acetone by means of high level ab initio methods. The calculations have been carried out on multiconfigurational self consistent field (MCSCF) level with a subsequent addition of dynamical correlation both by a perturbation theory (CASPT2) and via a configuration interaction expansion up to double excitations (MR-CISD). The major question we address is whether the dynamical processes occur adiabatically on the S_2 surface or diabatically, with non-adiabatic transitions taking place in the course of the reactions. To do so, we explore in detail the S_2/S_1 intersection space and all important transition states. We focus both on the Norrish type reaction and on the minor hydrogen dissociation channel.

Our second goal was to test the results with respect to decreasing the computational level by reducing the size of the basis set and of the active space as well as switching from the computationally demanding configuration interaction to the more cost-effective perturbation theory approach. Keeping the calculations relatively inexpensive is important for future dynamical studies on relatively long time scales.

COMPUTATIONAL METHODS

Important points on the potential energy surfaces (PES) of acetone, i.e. ground and excited states minima (denoted further on as MIN), transition states (TS) and minima on crossing seams between two or three electronic states (MXS) together with interpolation curves for reaction paths have been characterized. The ground state (S_0), the first (S_1) and the second excited singlet (S_2) states have been considered. Calculations were performed using two approaches differing in the active space, the basis set and the way of treating electronic correlation effects.

MR-CISD Calculations

In the first step, state averaged SA-MCSCF calculations with equal weights for three singlet states were performed in order to determine the molecular orbitals (MOs). Gas-phase frequencies were calculated at the MCSCF level of

theory by means of numerical differentiation of analytic gradients to determine the nature of the stationary point encountered. The basis set (denoted as 6-31+G(d)1s) was constructed from the 6-31+G(d) basis set by adding one more diffuse s functions on carbon (exponent 0.0138000, coefficient 1.0000) and oxygen (exponent 0.0281667, coefficient 1.0000) atoms, while for hydrogen atoms 6-31G(d) basis set was used.

The set of reference configuration state functions (CSFs) used in this calculation was constructed by including seven valence orbitals (n_O, π_{CO}, π_{CO}^* and two pairs of σ and σ^* orbitals) and eight electrons into the complete active space (CAS). Further, only single excitations were allowed from the CAS to the additional auxiliary 3s Rydberg (AUX) orbital. The final expansion space for the multireference configuration interaction method in terms of CSFs is constructed by allowing all single and double excitations (MR-CISD) from all reference configurations into all virtual orbitals. The reference spaces comprised five valence orbitals and six electrons and only the single excitation from n_O to the 3s Rydberg orbital is left in the reference space for the description of 3s Rydberg state. Furthermore, the four core orbitals have been kept frozen in all MR-CISD calculations.

Accordingly, acetyl radical was described by a valence CAS constructed from six orbitals and seven electrons. The reference space was reduced to four orbitals and five electrons and three core orbitals have been kept frozen in the MR-CISD calculations. In the case of stationary points on the S_2 potential energy surface of the acetyl radical, an additional n_O–σ_{CC}^* configuration was added to the reference space since a strong mixing of Rydberg and valence character of the wavefunction was noted in the region of the PES along the C–C dissociation reaction coordinate. The energies of the methyl radical and the hydrogen atom were calculated at the SCF and CISD levels of theory and added to the total energies of the acetyl and CH_3COCH_2 radicals calculated at MCSCF and MR-CISD levels of theory, respectively. Additionally, size-extensivity corrections were computed by means of the extended Davidson method (MR-CISD+Q)[16]. All structures were optimized without symmetry restrictions using direct inversion of iteration space for geometry optimization (GDIIS)[17] procedure. Harmonic vibrational frequencies were calculated by the suscal program[18]. All calculations at MCSCF and MR-CISD levels of theory have been performed with the COLUMBUS [19] suite of codes using its analytical gradient and nonadiabatic coupling vector features.

CASPT2 Calculations

As was already pointed out in the Introduction, the effect of decreasing computational efforts on the results will be analyzed. Therefore in the second approach, the 6-31+G(d) basis has been used for the multistate CASPT2 calculations. The active space consisted of six electrons in five orbitals. This active space is large enough to model all states of interest, i.e. the ground state, the $S_1(n,\pi^*)$ state and the $S_2(n,3s)$ state. A level shift of 0.4 hartree was applied. In order to keep a consistent active space, the whole potential energy surface was calculated at one computational level. Thus, properties of the acetyl radical were calculated keeping the dissociated methyl radical in a fixed distance of 8 Å. Local minima were obtained by standard minimization routines as implemented in the MOLPRO package[20]. Minima on the crossing seam were calculated using the CIOpt code[21]. Transition states were obtained via a constrained optimization procedure. The MOLPRO quantum chemistry package has been used for the CASPT2 calculation.

RESULTS AND DISCUSSION

We have considered three lowest-lying electronic states of acetone: the S_0 ground state, the S_1 state of (n,π^*) character and the S_2 Rydberg (n,3s) state. Excitation into the S_1 state corresponds to a promotion of an electron from a non-bonding orbital located on the oxygen atom to a π antibonding C–O orbital. As one could expect for this type of excitation, the corresponding band in the absorption spectrum is very weak. Acetone, on the other hand, absorbs strongly in the VUV region[22,23]. After irradiation with a 193 nm photon, the system is excited into the S_2 state which is of (n,3s) Rydberg character. The experimental vertical excitation energies were determined to be 4.49 and 6.36 eV [24] for the first and the second excited state, respectively. Our ab initio values calculated at the MR-CISD+Q and CASPT2 levels of theory (4.54 and 4.44 eV, respectively, for the first excited state and 6.55 and 6.65 eV, respectively, for the second excited state) are in good agreement with the measured values. This agreement assures that the vertical excitations are properly described by both approaches used. Next we shall turn to the characterization of the stationary points on the excited state PESs.

Geometries of all important points on the acetone PESs are shown in Fig. 1. In particular, the following structures are shown: ground state minimum (**MIN**($\mathbf{S_0}$)), S_1 minimum (**MIN**($\mathbf{S_1}$)), S_2 minimum (**MIN**($\mathbf{S_2}$)), TS for a CH_3 dissociation on the S_2 PES (**TS**$_{\mathbf{CC}}$($\mathbf{S_2}$)), TS for a hydrogen dissociation on

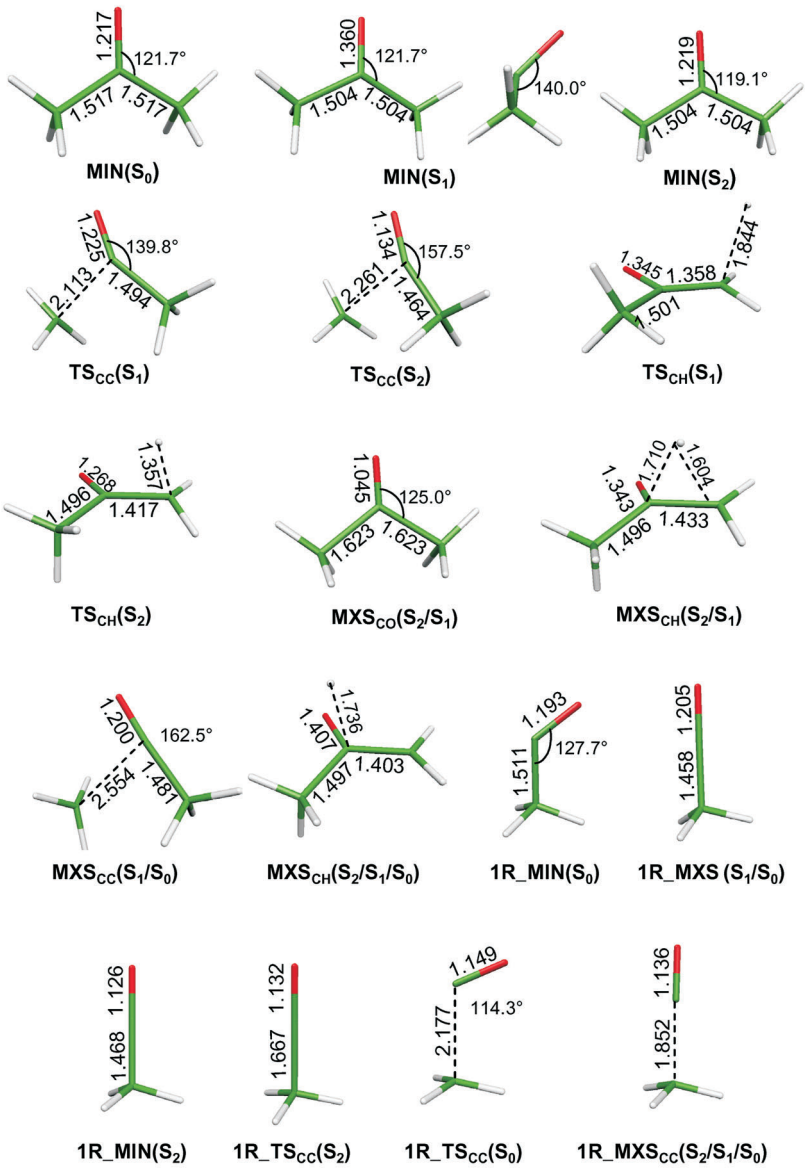

FIG. 1

Structures of stationary points on the S_0, S_1 and S_2 PESs of acetone calculated at the MR-CISD level of theory. The structure $\mathbf{MXS_{CH}(S_2/S_1/S_0)}$ was partially optimized at the MCSCF level of theory

the S_2 PES (**$TS_{CH}(S_2)$**), TS for a CH_3 dissociation on the S_1 PES (**$TS_{CC}(S_1)$**), TS for a CH_3 dissociation from the CH_3CO (S_2) fragment (**$1R\_TS_{CC}(S_2)$**), TS for a CH_3 dissociation from the CH_3CO (S_0) fragment (**$1R\_TS_{CC}(S_0)$**), a conical intersection between the S_2 and the S_1 states with a compressed C–O bond, **$MXS_{CO}(S_2/S_1)$**, and an intersection with a stretched CH bond, **$MXS_{CH}(S_2/S_1)$**), and three-state $S_2/S_1/S_0$ CIs for acetone and acetyl radical (**$MXS_{CH}(S_2/S_1/S_0)$** and **$1R\_MXS_{CC}(S_2/S_1/S_0)$**, respectively). The relative energies calculated with respect to the acetone ground state minimum at CASPT2 and MR-CISD+Q levels of theory are collected in Table I. Before dealing with deactivation processes upon photon absorption, we shall briefly discuss the adiabatic excitation energies. Fluorescence excitation experiments on a supersonic beam of acetone vapor gave an adiabatic energy of 3.774 eV [25] for the S_1 state. It is in good agreement to our calculated value of 3.74 eV at the MR-CISD+Q level of theory. The stabilization of the S_2 energy from the Franck–Condon point to the geometry structure of **$MIN(S_1)$** (0.8 eV) is attributed, mostly, to the strong C–O bond out of plane motion and is in accord to previous theoretical results[2,26]. The geometry of the S_2 excited state minimum (**$MIN(S_2)$**) is only slightly distorted with respect to the **$MIN(S_0)$** by means of in-plane internal coordinates: the C–O bond is stretched by 0.002 Å, the C–C bond is compressed by 0.013 Å and the C–C–C angle is increased by 5.2° (see Fig. 1). Therefore, the energy difference between the adiabatic and vertical excitation energy in the case of the S_2 excited state (0.08 eV) is ten times smaller than in the case of the S_1 state.

All considered processes upon the excitation into the 3s Rydberg state of acetone are schematically shown in Fig. 2. There are three reaction channels that system might use for deactivation: (i) methyl dissociation on the S_2 PES, (ii) S_2/S_1 internal conversion followed by either methyl (ii-a) or hydrogen (ii-b) dissociation in the S_1 state, and (iii) hydrogen dissociation and shift along the neighboring C–C bond on the S_2 PES followed by S_2/S_0 internal conversion via a three-state intersection. The mechanisms will be discussed in detail based on the MR-CISD structures and MR-CISD+Q calculated energies in next subsections. The comparison with the CASPT2 approach will be given in the most important points.

Methyl Dissociation

There are two possible pathways for the methyl dissociation. The adiabatic one (i) takes place only on the S_2 potential surface, while the diabatic mechanism, (ii-a) involves one internal conversion step before the acetone

TABLE I
Relative energies of stationary points on the acetone singlet PESs (ground state S_0, first and second excited states S_1 and S_2) with respect to the ground state minimum calculated by different theoretical methods. For corresponding geometries see Fig. 1

Stacionary point	MCSCF E_{rel}/eV	N_{Imag}	MR-CISD E_{rel}/eV	MR-CISD+Q E_{rel}/eV	CASPT2 E_{rel}/eV
MIN(S_0)[a]	–192.02586	0	–192.48955	–192.55736	–192.52721
MIN(S_1)	3.54	0	3.72	3.74	3.64
MIN(S_2)	6.17	0	6.77	6.47	6.52
$TS_{CC}(S_1)$	4.74	1	4.88	4.90	4.85
$TS_{CC}(S_2)$	6.51	1	7.50	7.11	7.30
$TS_{CH}(S_1)$	4.98	1	5.60	5.36	5.37
$TS_{CH}(S_2)$	7.15	1	7.43	7.19	7.21
$MXS_{CO}(S_2/S_1)$	6.85	–	8.45	8.23	7.84
$MXS_{CH}(S_2/S_1)$	6.73	–	6.97	6.96	6.91
$MXS_{CH}(S_2/S_1/S_0)$[b]	4.93	–	6.62	5.84	5.69
$MXS_{CC}(S_1/S_0)$	4.55	–	4.71	4.78	4.58
1R(S_2,linear) + CH_3[c]	5.92	0	6.09	6.29	[d]
1R_$TS_{CC}(S_2)$ + CH_3[c]	5.95	1	6.24	6.38	[d]
1R_$MXS_{CC}(S_2/S_1/S_0)$ + CH_3[e]	5.49	–	5.82	5.98	[d]
1R(S_0,linear) + CH_3[c]	4.71	1	4.19	4.75	5.02
1R(S_0,bent) + CH_3[c]	3.20	0	2.85	3.39	3.67
1R_$TS_{CC}(S_0)$ + CH_3[c]	3.65	1	4.06	4.14	4.56
2R(S_0) + H[f]	3.35	0	4.96	3.86	4.06
CO + 2 CH_3	2.76	0	2.45	3.56	4.36

[a] Total energies for ground state minimum are given in a.u. [b] MCSCF optimization of three-state conical intersection, energies computed at the MR-CISD and MR-CISD+Q levels from single point calculation. [c] The total energy of CH_3 radical calculated by the SCF (–39.55457 a.u.), SR-CISD (–39.68381 a.u.) and SR-CISD+Q (–39.69034 a.u.) methods and added to the total energy of acetyl radical (**1R**) at the MCSCF, MR-CISD and MR-CISD+Q levels of theory, respectively. [d] CASPT2 calculations for the S_2 electronic state of the acetyl radical are omitted as the respective active space is not suited for these calculations. [e] MCSCF and partial MR-CISD optimizations of three-state conical intersection as discussed in the text. [f] The total energy of hydrogen atom, calculated by SCF (–0.49823 a.u.), is added to the total energy of the acetonyl radical (**2R**).

cleavage is completed. Energy profiles for both possible mechanisms are shown in Fig. 3.

The transition state $\mathbf{TS_{CC}(S_2)}$ for α-CH_3 dissociation on the S_2 surface is located 0.64 eV above the S_2 minimum. The stretching of the C–C bond from 1.504 Å in the $\mathbf{MIN(S_2)}$ to 2.261 Å in the saddle point $\mathbf{TS_{CC}(S_2)}$ is accompanied by strong opening of the C–C–O angle from 119.1 to 157.5°. If we freeze the C–C–O angle at a value of 120°, the barrier would increase to 2.34 eV. Therefore it can be concluded that opening of the C–C–O angle is vital for keeping the dissociation barrier low. In other words, while the activation energy is reasonably low, the activation entropy will disfavor this reaction channel. The release of a second methyl group from the acetyl radical in the S_2 state is accompanied only by a negligible barrier of 0.09 eV (via a transition state $\mathbf{1R\_TS_{CC}(S_2)}$, see Fig. 3a). Further stretching of C–C bond leads the system to the three state conical intersection $\mathbf{1R\_MXS_{CC}(S_2/S_1/S_0)}$ where fast decay to the ground state occurs. The first methyl dissociation is the rate determining step for the adiabatic pathway.

The diabatic pathway (ii-a) (Fig. 3b) starts with a transfer of electronic population from the S_2 into the S_1 state. After dissociation of the methyl group on the S_1 PES, the acetyl radical can easily relax from the excited CH_3CO (S_1) state into its ground electronic state – the minimum for the S_1 state of the acetyl radical is at the same time the S_1/S_0 intersection. The dissociation of the second methyl radical occurs on the ground state PES.

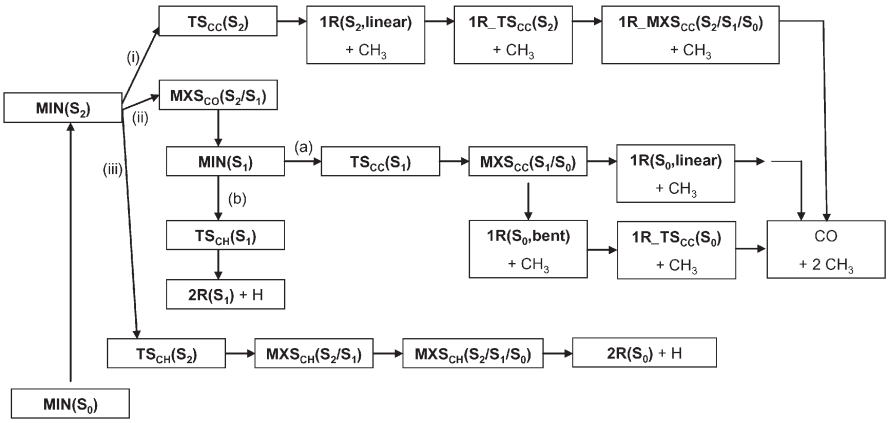

FIG. 2

Possible deactivation paths in acetone upon excitation to the S_2 excited state. Acetyl and acetonyl radicals are labeled with **1R** and **2R**, respectively

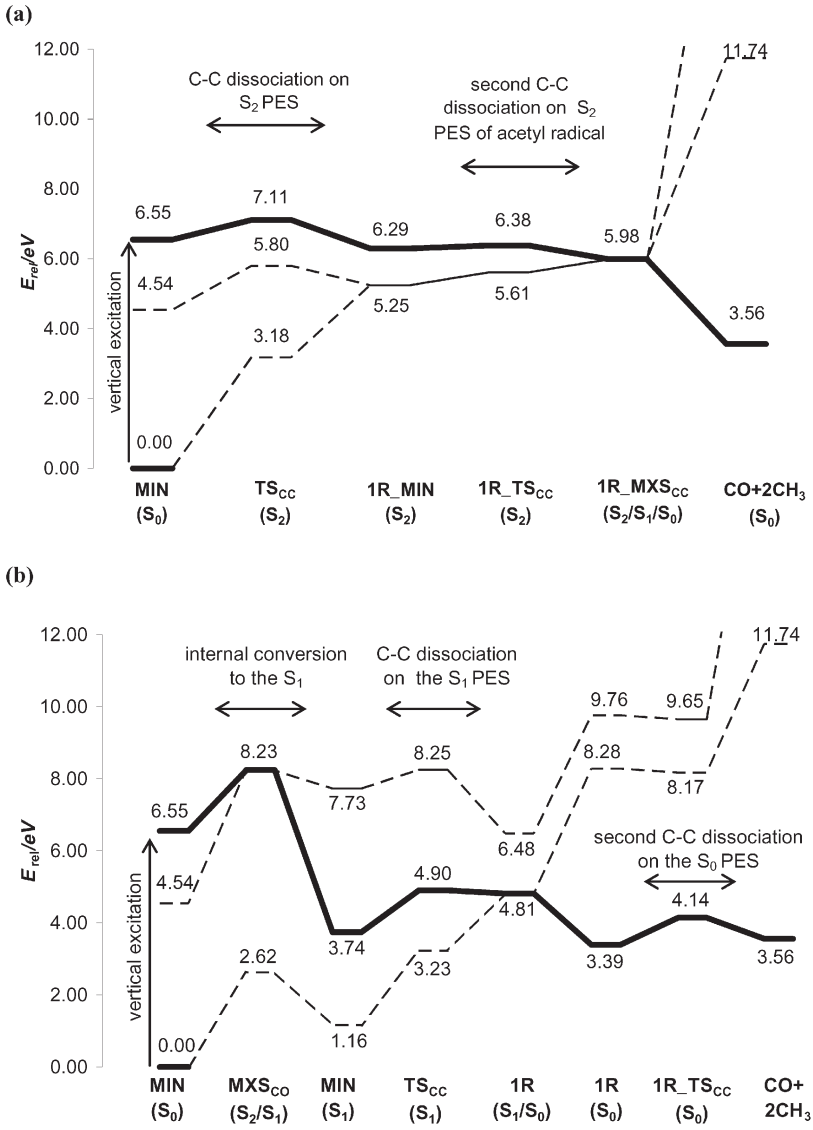

FIG. 3

Relative energies, with respect to the ground state, of the stationary points along the deactivation pathway a (i) and b (ii-a) of acetone upon excitation into the S_2 state leading to the formation of CO and methyl radicals. The energies are calculated at the MR-CISD+Q/6-31+G(d)1s level of theory

The population transfer from the S_2 to the S_1 excited state can be mediated via the C_{2v} conical intersection (here $\mathbf{MXS_{CO}(S_2/S_1)}$) that has been previously described by Diau et al.[4]. Its geometry is characterized by a very short C–O bond (1.045 Å) and symmetrically stretched C–C bonds (1.623 Å). The relative energy of the $\mathbf{MXS_{CO}(S_2/S_1)}$ with respect to the $\mathbf{MIN(S_0)}$ strongly depends on the applied method: 6.85, 8.23 and 7.84 eV calculated with MCSCF, MR-CISD+Q and CASPT2, respectively. Furthermore, a similar method dependent variation can be found also in the C–O bond distance (1.077, 1.045 and 1.081 Å at the MCSCF, MR-CISD and CASPT2 levels, respectively). The reason behind this discrepancy can be traced back to the topology of the conical intersection illustrated in the Fig. 4. The potential energy curve between the $\mathbf{MIN(S_0)}$ and the $\mathbf{MXS_{CO}(S_2/S_1)}$ structures have been calculated by linear interpolation of all internal coordinates. It is noted that the S_2 PES is relatively flat near the ground state geometry and that there is a very strong uphill character of the S_2 and S_1 PESs leading to the MXS. Therefore, a small change along the reaction coordinate brings a very large change in the energy of the intersection.

Based solely on energetic considerations, it can be concluded that the adiabatic methyl dissociation represents the major photodissociation path-

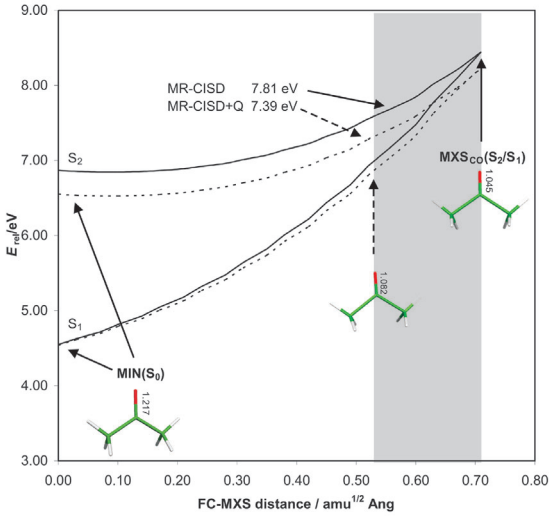

FIG. 4

Linear interpolation between the $\mathbf{MIN(S_0)}$ and $\mathbf{MXS_{CO}(S_2/S_1)}$ calculated at the MR-CISD (solid line) and MR-CISD+Q (dashed line) levels of theory. Gray area represents the space where the energy gap between S_1 and S_2 states is smaller than 0.4 eV at the MR-CISD+Q level

way due to the significantly smaller barrier (0.64 eV). This conclusion is however in a strong contradiction to the experimental findings since the direct dissociation mechanism is not supported by femtosecond experiments of Chen et al.[9]. It has been observed previously[27a] that the topography of the conical intersection (sloped versus peaked[27b,27c]) can result into a preference of one reaction channel. More generally, photodynamical processes are driven not only by energy of the conical intersection seam but also by entropy effects. It is clearly seen in Fig. 5 that the crossing seam almost isoenergetically extends in the direction of asymmetrical C–C stretch. It should be also mentioned that the asymmetrical conical intersections at the CASPT2 level with one of the C–C bonds at approximately the same length as in the S_0 minimum geometry (~1.54 Å) and the second one considerably stretched (~1.79 Å) are energetically lower than the energy of the symmetric one. Apparently, the $\mathbf{MXS_{CO}(S_2/S_1)}$ belongs to an almost isoenergetic intersection seam that spans a large portion of the configuration space in the direction of the CH_3 dissociation path. On the other side, the direct CH_3 dissociation transition state covers only a very limited part of the configurational space at low enough energies.

Additionally, it should be emphasized that the population transfer from the upper to the lower state does not occur only near the minimum energy conical intersection and it is not even needed to precisely match the exact

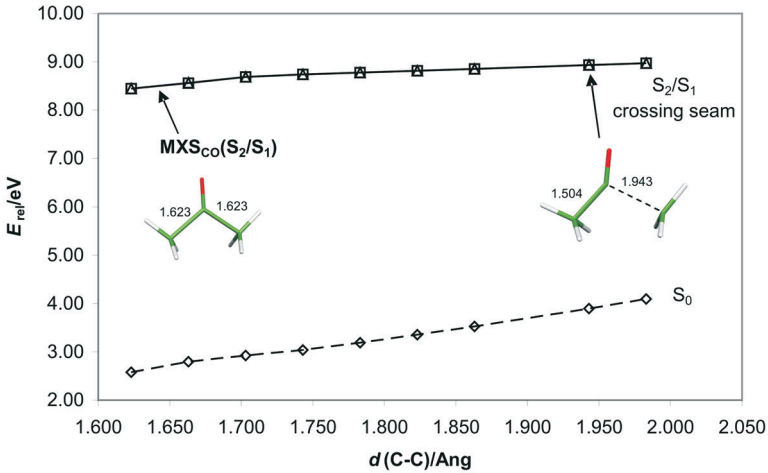

FIG. 5
Potential energy curve of the conical intersection seam (short C–O bond) along the C–C bond dissociation reaction. All points have been fully optimized with one C–C bond fixed

degeneracy point. It is both the energy difference and adiabatic coupling which effect probability of the transition into (lower) electronic state. Non-adiabatic dynamical calculations[12h,12j,28] demonstrate that even for such a rapid dynamical process as is the ethylene isomerization, population transfer typically occurs at energy gaps of several tenths of an eV. In the specific case of acetone, even larger energy gaps than in ethylene can be expected because of the aforementioned uphill character of the MXS slowing down the non-adiabatic transition considerably. Also the flatness of the S_2 potential near the Franck–Condon point allows the system to reach regions with a small S_2/S_1 gap with a lower energy than is needed to reach the $\mathbf{MXS_{CO}(S_2/S_1)}$. For example, the S_2/S_1 energy gap of 0.4 eV can be reached with an excess energy of 0.92 eV (Fig. 4). Our preliminary dynamical calculations at the MCSCF level[29] show that the population transfer from the S_2 to the S_1 state in acetone never proceeds via a point of an exact degeneracy. Instead, the population is gradually drained from the upper state to the lower state at a relatively low rate, corresponding to the picosecond timescale observed in the experiment.

Hydrogen Atom Dissociation

Similar to the methyl dissociation, we have also considered two dissociation mechanisms for hydrogen abstraction: an adiabatic cleavage on the S_2 potential surface (iii) and a diabatic pathway which includs relaxation into the S_1 state (ii) followed by the CH dissociation on the S_1 PES ((ii-b), Fig. 6).

A search along the C–H (out of plane hydrogen) reaction coordinate on the S_2 PES resulted in a transition structure $\mathbf{TS_{CH}(S_2)}$ 0.76 eV above the $\mathbf{MIN(S_2)}$ with a C–H distance of 1.357 Å. The dissociation of the C–H bond mostly affected the neighboring C–C bond and somewhat less the C–O bond: the length of the former was decreased by 0.087 Å and the latter one was increased by 0.049 Å (see Fig. 1). The remaining C–H bonds on the carbon atom in the reactive center moved into the plane of the C and O atoms. The most striking feature of the $\mathbf{TS_{CH}(S_2)}$ structure is the position of dissociated hydrogen atom. It is shifted above the C–C–O plane and inclined over the neighboring C–C bond leading to a very large decrease in the corresponding C–C–H angle (77.0°). A similar position of the hydrogen atom is found in the $\mathbf{MXS_{CH}(S_2/S_1)}$ structure. The C–H bond is further stretched by 0.247 Å (with respect to $\mathbf{TS_{CH}(S_2)}$) and the C–C–H angle is decreased to 68.3°. It follows straightforwardly that this conical intersection is directly related to a hydrogen dissociation and shift along the C–C bond.

There is also a structurally related three-state $S_2/S_1/S_0$ conical intersection $\mathbf{MXS_{CH}(S_2/S_1/S_0)}$ where the hydrogen atom gets closer to the central carbon atom, with a C–H distance of about 1.7 Å. It has been shown only recently that three-state conical intersections are sometimes involved in photodynamical processes[30]. It should be noted that the three state conical intersection has been calculated by the search algorithm of the COLUMBUS program for a two-state conical intersection seam by using non-adiabatic coupling vectors and gradients for the first and the third root and therefore it is only partially optimized. The energies of both of $\mathbf{MXS_{CH}(S_2/S_1)}$ and $\mathbf{MXS_{CH}(S_2/S_1/S_0)}$ intersections are lower than the energy of the $\mathbf{MXS_{CO}(S_2/S_1)}$. The three state $\mathbf{MXS_{CH}(S_2/S_1/S_0)}$ lies even lower than S_2 in FC point. However, acetone has to surmount the $\mathbf{TS_{CH}(S_2)}$ point on its way to the conical intersections. Since this transition state is constrained in the configurational space, reaching these two CIs is limited again by entropical factors. The two- and the three-state hydrogen transfer intersections are separated only by a small barrier lower than 0.1 eV on the S_2 state PES and without any barrier on the S_1 state. Therefore, if the acetone molecule is

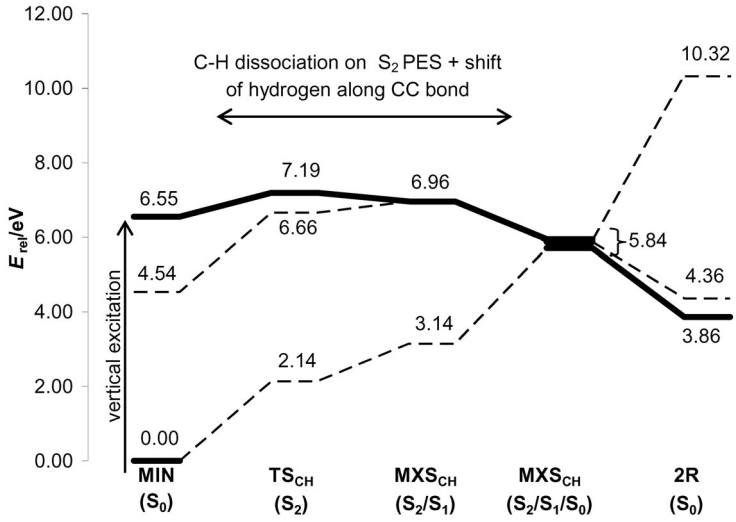

FIG. 6

Relative energies, with respect to the ground state, of the stationary points along the CH deactivation pathway (iii) of acetone upon excitation into the S_2 state leading to the formation of CO and methyl radicals. The energies are calculated at the MR-CISD+Q/6-31+G(d)1s level of theory

able to reach geometries close to $\mathbf{MXS_{CH}(S_2/S_1)}$ or $\mathbf{MXS_{CH}(S_2/S_1/S_0)}$, it directly moves to the S_0 ground state from which the hydrogen atom (at that moment very loosely bound to the carbonyl carbon atom) can readily dissociate. It is very interesting to note that the relative energies for all stationary points along reaction path (iii) calculated with CASPT2 approach are in a good agreement to MRCISD+Q values. They are slightly lowered with the largest discrepancy of 0.15 eV in the $\mathbf{MXS_{CH}(S_2/S_1/S_0)}$ point. This is not surprising since its MRCISD+Q energy is estimated as average energy of three roots in a single point calculation on partially optimized structure at the MCSCF level of theory.

As we have already suggested above, hydrogen atoms can be formed in the S_0 state after a direct internal conversion from the S_2 state via the three-state intersection $\mathbf{MXS_{CH}(S_2/S_1/S_0)}$. There is, however, still open possibility that the hydrogen atoms are formed in the S_1 state after the S_2/S_1 internal conversion via the $\mathbf{MXS_{CO}(S_2/S_1)}$ intersection seam which is involved in the diabatic methyl dissociation mechanism (ii). Therefore, a search along the CH dissociation path on the S_1 PES of acetone was carried out. The transition structure for the (ii-a) path possesses a strongly stretched C–H bond of 1.844 Å. It should be pointed out that its length is 0.487 Å longer than the corresponding C–H bond in $\mathbf{TS_{CH}(S_2)}$. Also the C–C–H angle is not inclined over the neighboring C–C bond but is widely opened (106.1°). The energy barrier for the hydrogen dissociation on the S_1 PES is 0.46 eV larger than the barrier for methyl dissociation. Therefore hydrogen dissociation from the S_1 state is energetically less favorable than methyl dissociation. This conclusion is consistent with experiments where acetonyl radical (**2R**) is observed as a minor photoproduct[13].

CONCLUSIONS

The photolysis of acetone upon excitation into the 3s Rydberg state (the S_2 state) has been investigated by means of high-level ab initio calculations (MCSCF, CASPT2 and MR-CISD+Q). The major photoproducts (CO and two methyl radicals) are formed via stepwise cleavage of both C–C bonds. The dissociation of the α-CC bond can be accomplished either on the S_2 PES (adiabatically) or following the internal conversion in the S_1 state (diabatically).

In order to compare both possible reaction pathways and decay mechanisms all relevant structures on the acetone PESs have been characterized by two different approaches: MR-CISD+Q and CASPT2. Both approaches are in quite satisfactory agreement for most of the examined stationary points.

However, from our calculations of the excited energies alone it was very difficult to decide along which pathway the system might decay. To overcome this problem, the discussion on the topology and spatial extension of the key points in the reaction paths was also included. We concluded that the acetone cleavage most likely takes place on the S_1 surface, preceded by a non-adiabatic transfer from S_2 to S_1. Finally, it should be emphasized that the results obtained with our higher level approach fully support the previous mechanism for the Norrish type cleavage obtained by less sophisticated CASSCF(6,7)/6-311+G(d,p) approach of Diau et al.[4].

In addition to the major photoreaction, formation of hydrogen and acetonyl (or 1-methyloxy or 2-oxopropyl) radical has been discussed. Similarly as for the methyl dissociation, we have also considered two dissociation mechanisms. In an adiabatic mechanism, the cleavage of the C–H bond starts on the S_2 potential surface and the hydrogen is simultaneously shifted along the neighboring C–C bond. When the system overcomes the energy barrier for the dissociation, very fast decay to the S_1 and the ground state is expected due to the presence of two state and three state conical intersections with structures similar to the $\mathbf{TS_{CH}(S_2)}$. The diabatic pathway for CH dissociation starts with population transfer from S_2 to the S_1 state. In the next step the dissociation of the C–H bond occurs on the first excited state potential energy surface where it competes with the major methyl dissociation channel (a). The hydrogen dissociation on the S_1 PES is energetically less favorable but still energetically accessible.

It should be emphasized that the preferred reaction mechanism can not be suggested solely on the basis of single point energy calculations. It seems that the photodynamics of acetone is not primarily dictated by the energetics, the importance of different reaction channels is changed upon consideration of entropical factors. The role of entropical on non-adiabatic processes deserves further exploration, e.g. analyzing the conical intersection curvature[31] or by the constrained molecular dynamics[32]. To ultimately resolve the problem which of the proposed reaction channels is dominant, ab initio dynamical simulations have to be performed. Such studies are possible now and ab initio dynamics has been proven to successfully resolve several photodynamical problems[33].

The authors acknowledge support of the Ministry of Education, Youth and Sports of the Czech Republic (research project No. 6046137307 and Czech-American cooperation grant ME08086), the Austrian Science fund within the framework of the Special Research Program F16 (P18411-N19), the WTZ treaty between Austria and Croatia (HR17/2008), the Ministry of Science, Education and Sport of Croatia (Project No. 098-0982933-2920) and the COST D37 action, WG0001-06. The

calculations were performed in part on the Schroedinger III Linux cluster of the Vienna University Computer Centre and on computer cluster of Center for complex molecular systems (project LC512).

REFERENCES

1. For recent review see: Haas Y.: *Photochem. Photobiol. Sci.* **2004**, *3*, 6.
2. a) Blitz M. A., Heard D. E., Pilling M. J.: *J. Phys. Chem. A* **2006**, *110*, 6742; b) Somnitz H., Fida M., Ufer T., Zellner R.: *Phys. Chem. Chem. Phys.* **2005**, *7*, 3342; c) Kim S. K., Pedersen S., Zewail A. H.: *J. Chem. Phys.* **1995**, *103*, 477; d) Waits L. D., Horwitz R. J.: *Chem. Phys.* **1991**, *155*, 149; e) Zuckermann H., Schmitz B., Haas Y.: *J. Phys. Chem.* **1988**, *92*, 4835; f) Zuchermann H., Schmitz B., Haas Y.: *Chem. Phys. Lett.* **1988**, *151*, 323; g) Zuchermann H., Haas Y., Drabbels M., Heinze J., Meerts W. L., Reuss J., Vanbladel J.: *Chem. Phys.* **1992**, *163*, 193
3. Diau E. W.-G., Kötting C., Zewail A. H.: *ChemPhysChem* **2001**, *2*, 273.
4. Diau E. W.-G., Kötting C., Sølling T. I., Zewail A. H.: *ChemPhysChem* **2002**, *3*, 57.
5. Sølling T. I., Diau E. W.-G., Kötting C., De Feyter S., Zewail A. H.: *ChemPhysChem* **2002**, *3*, 79.
6. Zhong Q., Steinhurst D. A., Baronavski A. P., Owrutsky J. C.: *Chem. Phys. Lett.* **2003**, *370*, 609.
7. a) Nádasdi R., Kovács G., Szilágyi I., Demeter A., Dóbé S., Bérces T., Márta F.: *Chem. Phys. Lett.* **2007**, *440*, 31; b) Jaeglé L., Jacob D. J., Brune W. H., Wennberg P. O.: *Atmos. Environ.* **2001**, *35*, 469; c) Wennberg P. O., Hanisco T. F., Jaeglé L., Jacob D. J., Hintsa E. J., Lanzendorf E. J., Anderson J. G., Gao R.-S., Keim E. R., Donnelly S. G., Del Negro L. A., Fahey D. W., McKeen S. A., Salawitch R. J., Webster C. R., May R. D., Herman R. L., Proffitt M. H., Margitan J. J., Atlas E. L., Schauffler S. M., Flocke F., McElroy C. T., Bui T. P.: *Science* **1998**, *279*, 49; d) McKeen S. A., Gierzak T., Burkholder J. B., Wennberg P. O., Hanisco T. F., Keim E. R., Gao R.-S., Liu S. C., Ravishankara A. R., Fahey D. W.: *Geophys. Res. Lett.* **1997**, *24*, 3177; e) Singh H. B., Kanakidou M., Crutzen P. J., Jacob D. J.: *Nature* **1995**, *378*, 50.
8. a) Owrutsky J., Baronavski J.: *J. Chem. Phys.* **1998**, *108*, 6652; b) Owrutsky J., Baronavski A.: *J. Chem. Phys.* **1999**, *110*, 11206; c) North S. W., Blank D. A., Gezelter J. D., Longfellow C. A., Lee Y. T.: *J. Chem. Phys.* **1995**, *102*, 4448; d) Zhong Q., Poth L., Castleman A. W., Jr.: *J. Chem. Phys.* **1999**, *110*, 192; e) Trentelman K. A., Kable S. H., Moss D. B., Houston P. L.: *J. Chem. Phys.* **1989**, *91*, 7498; f) Donaldson D. J., Gaines G. A., Vaida V.: *J. Chem. Phys.* **1988**, *92*, 2766; g) Donaldson D. J., Leone S. R.: *J. Chem. Phys.* **1986**, *85*, 817.
9. a) Chen W., Ho J., Cheng P.: *J. Phys. Chem. A* **2005**, *109*, 6805; b) Chen W., Ho J., Cheng P.: *Chem. Phys. Lett.* **2003**, *380*, 411; c) Chen W., Cheng P.: *J. Phys. Chem. A* **2005**, *109*, 6818.
10. Chen W., Ho J., Cheng P.: *Chem. Phys. Lett.* **2005**, *416*, 291.
11. Khamaganov V., Karunanandan R., Rodriguez A., Crowley J. N.: *Phys. Chem. Chem. Phys.* **2007**, *9*, 4098.
12. a) Antol I., Vazdar M., Barbatti M., Eckert-Maksić M.: *Chem Phys.* **2008**, *349*, 308; b) Barbatti M., Ruckenbauer M., Szymczak J. J., Aquino A. J. A., Lischka H.: *Phys. Chem. Chem. Phys.* **2008**, *10*, 482; c) Barbatti M., Lischka H.: *J. Am. Chem. Soc.* **2008**, doi: 10.1021/ja800589p; d) Barbatti M., Sellner B., Aquino A. J. A., Lischka H. in: *Radiation Induced Molecular Phenomena in Nucleic Acid* (M. K. Shukla and J. Leszczynski, Eds),

p. 209. Springer, Netherlands 2008; e) Antol I., Eckert-Maksić M., Barbatti M., Lischka H.: *J. Chem. Phys.* **2007**, *127*, 234303; f) Barbatti M., Lischka H.: *J. Phys. Chem. A* **2007**, *111*, 2852; g) Antol I., Barbatti M., Eckert-Maksić M., Lischka H.: *Chem. Monthly* **2008**, *139*, 319; h) Barbatti M., Ruckenbauer M., Lischka H.: *J. Chem. Phys.* **2005**, *122*, 174307; i) Schubert B., Köppel H., Lischka H.: *J. Chem. Phys.* **2005**, *122*, 184312; j) Barbatti M., Granucci G., Persico M., Lischka H.: *Chem. Phys. Lett.* **2005**, *401*, 276; k) Antol I., Eckert-Maksić M., Lischka H.: *J. Phys. Chem. A* **2004**, *108*, 10317; l) Antol I., Eckert-Maksić M., Müller Th., Dallos M., Lischka H.: *Chem. Phys. Lett.* **2003**, *374*, 587.

13. Lightfoot P. D., Kirwan S. P., Pilling M. J.: *J. Phys. Chem.* **1988**, *92*, 4938.
14. Washida N., Inomata S., Furubayashi M.: *J. Phys. Chem. A* **1998**, *102*, 7924.
15. Takahashi K., Nakayama T., Matsumi Y., Osamura Y.: *J. Phys. Chem. A* **2004**, *108*, 8002.
16. a) Langhoff S. R., Davidson E. R.: *Int. J. Quantum. Chem.* **1974**, *8*, 61; b) Bruna P. J., Peyerimhoff S. D., Buenker R. J.: *Chem. Phys. Lett.* **1981**, *72*, 278.
17. Császár P., Pulay P.: *J. Mol. Struct.* **1984**, *114*, 31.
18. Pulay P., Fogarasi G., Pongor G., Boggs J. E., Vargha A.: *J. Am. Chem. Soc.* **1983**, *105*, 7037.
19. a) Lischka H., Shepard R., Pitzer R. M., Shavitt I., Dallos M., Müller T., Szalay P. G., Seth M., Kedziora G. S., Yabushita S., Zhang Z.: *Phys. Chem. Chem. Phys.* **2001**, *3*, 664; b) Shepard R., Shavitt I., Pitzer R. M., Comeau D. C., Pepper M., Lischka H., Szalay P. G., Ahlrichs R., Brown F. B., Zhao J.: *Int. J. Quantum Chem., Quantum Chem. Symp.* **1988**, *22*, 149; c) Shepard R., Lischka H., Szalay P. G., Kovar T., Ernzerhof M.: *J. Chem. Phys.* **1992**, *96*, 2085; d) Lischka H., Dallos M., Shepard R.: *Mol. Phys.* **2002**, *100*, 1647; e) Lischka H., Dallos M., Szalay P. G., Yarkony D. R., Shepard R.: *J. Chem. Phys.* **2004**, *120*, 7322; f) Dallos M., Lischka H., Shepard R., Yarkony D. R., Szalay P. G.: *J. Chem. Phys.* **2004**, *120*, 7330; g) Lischka H., Shepard R., Shavitt I., Pitzer R. M., Dallos M., Müller Th., Szalay P. G., Brown F. B., Ahlrichs R., Böhm H. J., Chang A., Comeau D. C., Gdanitz R., Dachsel H., Ehrhardt C., Ernzerhof M., Höchtl P., Irle S., Kedziora G., Kovar T., Parasuk V., Pepper M. J. M., Scharf P., Schiffer H., Schindler M., Schüler M., Seth M., Stahlberg E. A., Zhao J.-G., Yabushita S., Zhang Z.: *COLUMBUS, An ab initio Electronic Structure Program*. Release 5.9, 2001.
20. Werner H.-J., Knowles P. J., Lindh R., Manby F. R., Schütz M., Celani P., Korona T., Rauhut G., Amos R. D., Bernhardsson A., Berning A., Cooper D. L., Deegan M. J. O., Dobbyn A. J., Eckert F., Hampel C., Hetzer G., Lloyd A. W., McNicholas S. J., Meyer W., Mura M. E., Nicklaß A., Palmieri P., Pitzer R., Schumann U., Stoll H., Stone A. J., Tarroni R., Thorsteinsson T.: *MOLPRO, A Package of ab initio Programs*.
21. Levine B. G., Coe J. D., Martínez T. J.: *J. Phys. Chem. B* **2008**, *112*, 405.
22. Philis J., Goodman L.: *J. Chem. Phys.* **1993**, *98*, 3795.
23. Walzl K., Koerting C., Kuppermann A.: *J. Chem. Phys.* **1987**, *87*, 3796.
24. Nobre M., Fernandes A., da Silva F. F., Antunes R., Almeida D., Kokhan V., Hoffmann S. V., Mason N. J., Eden S., Limao-Vieira P.: *Phys. Chem. Chem. Phys.* **2008**, *10*, 550.
25. Baba M., Hanazaki I., Nagashima U.: *J. Chem. Phys.* **1985**, *82*, 3938.
26. Liu D., Fang W.-H., Fu X.-Y.: *Chem. Phys. Lett.* **2000**, *325*, 86.
27. a) Ben-Nun M., Molnar F., Schulten K., Martínez T. J.: *Proc. Natl. Acad. Sci. U.S.A.* **2002**, *99*, 1769; b) Atchity G. J., Xantheas S. S., Ruedenberg K.: *J. Chem. Phys.* **1991**, *95*, 1862; c) Yarkony D. R.: *J. Chem. Phys.* **2001**, *114*, 2601.
28. Levine B. G., Martínez T. J.: *Ann. Rev. Phys. Chem.* **2007**, *58*, 613.
29. Ončák M.: Unpublished results.

30. a) Matsika S., Yarkony D. R.: *J. Am. Chem. Soc.* **2003**, *125*, 10672; b) Matsika S., Yarkony D. R.: *J. Am. Chem. Soc.* **2003**, *125*, 12428; c) Coe J. D., Martínez T. J.: *J. Phys. Chem. A* **2006**, *110*, 618; d) Blancafort L., Robb M. A.: *J. Phys. Chem. A* **2004**, *108*, 10609.
31. Paterson M. J., Bearpark M. J., Robb M. A., Blancafort L.: *J. Chem. Phys.* **2004**, *124*, 11562.
32. Laino T., Passerone D.: *Chem. Phys. Lett.* **2004**, *389*, 1.
33. a) Muchová E., Slavíček P., Sobolewski A. L., Hobza P.: *J. Phys. Chem. A* **2007**, *111*, 5259; b) Barbatti M., Aquino A. J. A., Lischka H.: *Mol. Phys.* **2006**, *104* 1053; c) Mitrić R., Bonačić-Koutecký V., Pittner J., Lischka H.: *J. Chem. Phys.* **2006**, *125* 024303; d) Robb M. A., Garavelli M., Olivucci M., Bernardi F.: *Rev. Comput. Chem.* **2002**, *15*, 87; e) Ben-Nun M., Martínez T. J.: *Chem. Phys. Lett.* **1998**, *298*, 57; f) Worth G. A., Robb M. A.: *Adv. Chem. Phys.* **2002**, *124*, 355; g) Hudock H. R., Levine B. G., Thompson A. L., Satzger H., Townsend D., Gador N., Ullrich S., Stolow A., Martínez T. J.: *J. Phys. Chem. A* **2007**, *111*, 8500; h) Kim M. H., Shen L., Tao H., Martínez T. J., Suits A. G.: *Science* **2007**, *315*, 1561.